ELSEVIER

Pressure and flow distribution in internal gas manifolds of a fuel-cell stack

Joon-Ho Koh, Hai-Kyung Seo, Choong Gon Lee,
Young-Sung Yoo, Hee Chun Lim[*]

*Advanced Energy and Technology Group, Korea Electric Power Research Institute,
103-16 Munji-dong, Yuseong-gu, Daejeon 305-380, South Korea*

Abstract

Gas-flow dynamics in internal gas manifolds of a fuel-cell stack are analyzed to investigate overall pressure variation and flow distribution. Different gas-flow patterns are considered in this analysis. Gas-flow through gas channels of each cell is modeled by means of Darcy's law where permeability should be determined on an experimental basis. Gas-flow in manifolds is modeled from the macroscopic mechanical energy balance with pressure-loss by wall friction and geometrical effects. A systematic algorithm to solve the proposed flow model is suggested to calculate pressure and flow distribution in fuel-cell stacks. Calculation is done for a 100-cell molten carbonate fuel-cell stack with internal manifolds. The results show that the pressure-loss by wall friction is negligible compared with the pressure recovery in inlet manifolds or loss in outlet manifolds due to mass dividing or combining flow at manifold–cell junctions. A more significant effect on manifold pressure possibly arises from the geometrical manifold structure which depends on the manifold size and shape. The geometrical effect is approximated from pressure-loss coefficients of several types of fittings and valves. The overall pressure and flow distribution is significantly affected by the value of the geometrical pressure-loss coefficient. It is also found that the flow in manifolds is mostly turbulent in the 100-cell stack and this way result in an uneven flow distribution when the stack manifold is incorrectly, designed.
© 2003 Elsevier Science B.V. All rights reserved.

Keywords: Fuel-cell; Stack; Manifold; Gas pressure; Flow distribution

1. Introduction

One of the engineering problems encountered in the design of fuel-cell stacks is the configuration of gas-flow manifolds and the overall pattern of gas-flow that would give uniform flow distribution and stable cell operation. The geometrical structure and size of the gas manifolds are the important parameters to be considered.

For planar-type fuel-cell stacks, it is first necessary to decide whether internal or external manifolds are to be used. External manifolds are simpler and less costly than internal manifolds, but there is a major drawback of gas leakage and sealing [1]. External manifolds also work only for a cross-type gas-flow configuration. Internal manifolds are often advantageous not only because of better sealing, but also because the stack is not sensitive to a change in height due to shrinking. In a molten carbonate fuel-cell (MCFC) stack, for example stack height changes significantly as the temperature

rises from room temperature to its operating condition (650 °C) because of shrinking of matrix layers. In this respect, internal manifolds are more practical than external designs. Shrinking may not be significant for solid oxide or polymer electrolyte membrane fuel-cell stacks, but the internal manifold design is usually favored for these fuel-cells because it allows more versatility in gas-flow configuration.

The geometrical design factors of internal manifold stacks include manifold structure, size, number of manifolds, overall gas-flow pattern, gas channel depth, active area for electrode reactions, and so on. The shapes of manifold holes can be circular, rectangular, or oblong. The cross-sectional area of the holes is important because it determines the linear velocity of gas-flow through the manifolds for a given flow rate of the inlet gas. The overall gas-flow pattern consists of several different flow components, namely inlet manifold flow, flow through channels on the electrodes, and outlet manifold flow. Usually, the flow pattern can be either a U-shape (reverse flow) where the outlet gas flows in opposite direction to the inlet gas, or a Z-shape (parallel flow) where the directions of the inlet and outlet gas-flows are the same

---
[*] Corresponding author. Tel.: +82-42-865-5390; fax: +82-42-865-5374.
E-mail address: fclim@kepri.re.kr (H.C. Lim).

Nomenclature

A_x	cross-section area of gas-flow channel on electrodes (m^2)
D	diameter of pipe (m)
D_H	hydraulic diameter of manifold hole (m)
f	fanning friction factor
F_r	force exerted by fluid during motion (N m^{-2})
g	gravitational acceleration constant (=9.8 m s^{-2})
h	height (m)
k	permeability (m^2)
K_f	geometrical pressure-loss coefficient
l_{wf}	friction loss in mechanical energy balance (m^2 s^{-2})
L	length of pipe (m)
L_e	equivalent cell-to-cell length in manifold flow region (m)
L_x	length of electrodes in fuel-cell stack (m)
N	number of cells in a stack
P_{exit}	exit pressure at outlet manifold (N m^{-2})
$\Delta P(i)$	pressure-change across the ith cell (N m^{-2})
$P(i)$	local gas dynamic pressure at the ith cell (N m^{-2})
$q_x(i)$	gas-flow rate in the ith cell channel (m^3 s^{-1})
Q_F	total feed gas-flow rate (m^3 s^{-1})
$Q(i)$	cumulative gas-flow rate in the ith manifolds (m^3 s^{-1})
$Re(i)$	Reynolds number at the ith cell
$u(i)$	gas linear velocity at the ith cell (m s^{-1})

Greek letters

$\alpha(i)$	pressure distribution factor for ith cell, defined in Eq. (21)
ε	tolerance for calculation error
η	viscosity (kg m^{-1} s^{-1})
ρ	density (kg m^{-3})
τ_s	shear stress (N m^{-2})

Superscripts

adj	adjusted value during inner loop of calculation
new	newly calculated value for next iteration step

Subscripts

in	inlet manifolds
out	outlet manifolds
ref	reference cell
x	coordinate of flow through cell channel
y	coordinate of flow through manifolds

(Fig. 1). In both cases, the inlet and outlet manifold flows are perpendicular to the gas-flow through the channels on the electrodes. Other types of flow pattern may also be possible.

It is often emphasized in fuel-cell stack design that pressure-change in manifolds should be much lower than
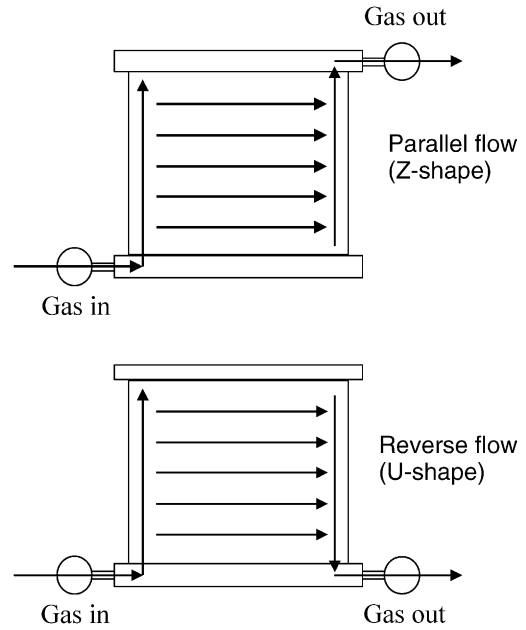

Fig. 1. Schematic of two different types of gas-flow pattern in fuel-cell stacks.

that in the gas channels on the electrodes in order to ensure a uniform flow distribution among cells piled in a stack. This rule-of-thumb is often satisfied when the number of cells in a single stack is not too large. There is no general design rule, however, as to how many cells are allowed to make a single stack with a reasonably good flow distribution. There have not been many large-scale stacks tested with near 100-cells in a single stack. One of the reasons for this paucity of test results is that fuel-cell stack construction is too costly to undertake mainly for the purpose of a pilot-scale engineering test. Theoretical approaches are therefore favored in the engineering design of fuel-cell stacks. It is the purpose of this paper to suggest a method to calculate the pressure variation for each directional component of gas-flow in planar type fuel-cell stacks in relation to flow distribution among the individual cells. There have been a few related studies in recent years [2–9], but we propose a more systematic algorithm for calculation. A specific case is illustrated by applying the proposed method for a pilot-scale fuel-cell stack.

2. Mathematical model

2.1. Number of variables and degree of freedom for analysis

Two overall flow patterns in fuel-cell stacks with planar cells are depicted in Fig. 1. The U-shape gas-flow may be called a 'reverse flow' as the outlet gas-flows in opposite direction to the inlet flow. The Z-shape gas-flow is a 'parallel flow' since both inlet and outlet gases flow in the same direction. Let us consider a stack where cells are numbered
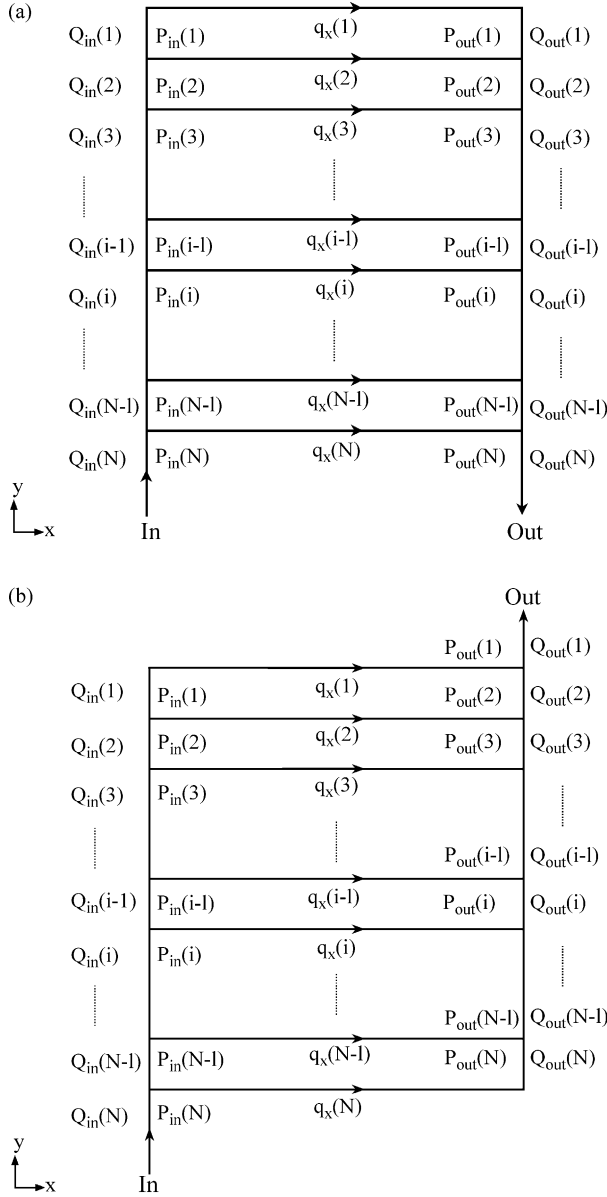
Fig. 2. Designation of pressure and flow variables for mathematical model: (a) reverse flow, (b) parallel flow.

from the highest (1st) to the lowest (Nth) position and the feed gas enters the Nth cell as shown in Fig. 2a for a reverse flow and in Fig. 2b for a parallel flow. The gas-flow in each cell through the channel area is denoted by $q_x(i)$. The dynamic pressure drop from the inlet to the outlet of a gas channel is denoted by $\Delta P_x(i)$ which must be a function of cell flow rate, i.e.

$$\Delta P_x(i) = P_{in}(i) - P_{out}(i), \quad (i = 1, 2, 3, \ldots, N) \qquad (1)$$

In inlet manifolds, the cumulative flow rate, $Q_{in}(i)$, and the local pressure drop, $\Delta P_{in}(i)$, are defined as follows:

$$Q_{in}(i) = \sum_{j=1}^{i} q_x(j) = Q_{in}(i-1) + q_x(i) \qquad (2)$$

$$Q_{in}(N) = Q_F \qquad (3)$$

where Q_F = total inlet feed flow rate.

$$\Delta P_{in}(i) = P_{in}(i) - P_{in}(i-1), \quad (i = 2, 3, \ldots, N) \qquad (4)$$

In outlet manifolds of a U-shape gas-flow stack, $Q_{out}(i)$ and $\Delta P_{out}(i)$ are defined as follows:

$$Q_{out}(i) = \sum_{j=1}^{i} q_x(j) = Q_{out}(i-1) + q_x(i) \qquad (5)$$

$$\Delta P_{out}(i) = P_{out}(i-1) - P_{out}(i), \quad (i = 2, 3, \ldots, N) \qquad (6)$$

In outlet manifolds of a Z-shape gas-flow stack, the same variables are given by:

$$Q_{out}(i) = \sum_{j=1}^{N} q_x(j) = Q_{out}(i+1) + q_x(i) \qquad (7)$$

$$\Delta P_{out}(i) = P_{out}(i) - P_{out}(i-1), \quad (i = 2, 3, \ldots, N) \qquad (8)$$

From Fig. 2, note that the total inlet flow rate is $Q_{in}(N)$ in both flow types while the total outlet flow rate is $Q_{out}(N)$ in a U-shape flow and $Q_{out}(1)$ in a Z-shape flow.

For an N-cell stack, there are $5N + 1$ variables involved to represent local pressure and flow rate, viz. $P_{in}(i)$, $P_{out}(i)$, $Q_{in}(i)$, $Q_{out}(i)$, $q_x(i)$, and Q_F. Among them, $Q_{in}(i)$ and $Q_{out}(i)$ are related directly to $q_x(i)$ from the $2N$ mass balance equations (Eqs. (2), (5) and (7)). A feed flow rate (Q_F) should be given as one of the operating parameters. To solve the given set of equations, therefore, requires $3N$ independent equations that relate local pressure and cell flow rate, $q_x(i)$. Two relations are pre-determined because $Q_{in}(N)$ is equal to the feed flow rate (Q_F) and the exit pressure must be known. The exit pressure is $P_{out}(N)$ for a U-shape flow and $P_{out}(1)$ for a Z-shape flow. The exit pressure is usually set to zero for dynamic pressure calculations. There should be $(N - 1)$ equations for $\Delta P_{in}(i)$ and another $(N - 1)$ equations for $\Delta P_{out}(i)$. In addition, N equations can be obtained from a relationship between cell flow rate, $q_x(i)$, and pressure drop, $\Delta P_x(i)$. Once all these relationships are defined, the degree of freedom becomes zero and thus the system can be solved to obtain flow and pressure distributions inside the manifolds and the cell channels.

2.2. Relation for cell flow rate and pressure drop

The gas-flow in cell channels can be approximated to a flow through a conduit for which many fluid dynamics relations are available as a function of the Reynolds number. Therefore, a flow model can be formulated to describe the gas-flow in cell channels. During operation under a current load, the mass flow rate varies from channel inlet to channel outlet as a result of consumption or generation by cell reactions. Such changes in mass flow should be accommodated in the flow model when gas utilization is high. When gas utilization is low, however, such a change of mass is not significant. The change of mass is not included in the model

explained below, but it can be easily added to the model equations with some modification. The treatment of mass change due to cell reactions has been reported in a study of fuel-cell performance models [10].

The gas-flow area on electrodes is often not straight channels but includes some regularly shaped obstacles for effective flow dispersion. These obstacles cause more flow resistance and, consequently, a higher pressure drop than straight open channels. The pressure drop in the gas channels is therefore strongly dependent on the shape and the configuration of the flow obstacles. A system-dependent parameter is necessary for the flow model in cell channels to absorb the effect of flow obstacles in gas channel area. Since the flow in a cell channel is usually in a laminar region, a linear relation of ΔP with flow rate should be reasonably satisfactory. A model of the cell channel flow can be derived from the Hagen–Poiseullie equation, Darcy's law, or others. Here, Darcy's law is used in which permeability (k) is the parameter that accounts for the flow resistance of the channel area,

$$\frac{\mathrm{d}P}{\mathrm{d}x} = -\eta \frac{u_x}{k} \tag{9}$$

Assuming gas viscosity and velocity are constants, the pressure drop from the inlet to the outlet is represented as follows:

$$\int_{\text{out}}^{\text{in}} \mathrm{d}P = -\eta \frac{u_x}{k} \int_{x=L_x}^{x=0} \mathrm{d}x \tag{10}$$

$$\Delta P_x(i) = P_{\text{in}}(i) - P_{\text{out}}(i) = \eta \frac{u_x(i)}{k} L_x \tag{11}$$

It is necessary to determine the permeability from measurement, and then the pressure drop from each cell channel is obtained directly from the linear gas velocity at the ith cell, $u_x(i)$.

2.3. Relation for manifold pressure and flow rate

The flow in manifolds is described quite differently from the flow in cell channels. In inlet manifolds, the gas-flow rate decreases from the feeding position to the other end. In outlet manifolds, the gas flow rate increases as the flow from each cell channel is sequentially added to the main flow. The overall gas-flow in manifolds is characterized by manifold axial flow (u_y) in combination with local dynamic pressure (P). A mathematical model for the gas pressure in manifolds is developed from an overall mechanical energy balance, or the engineering Bernoullie equation. Local velocities in the mechanical balance equation are related to mass or volumetric flow rates, which must be conserved from mass balances, i.e.

$$\frac{\Delta u_y^2}{2} + g\Delta h + \frac{\Delta P}{\rho} = l_{\text{wf}} \tag{12}$$

The friction loss term (l_{wf}) includes wall friction loss with a wall friction coefficient (f) which is defined as a ratio of

shear stress to inertial stress, i.e.

$$\frac{\text{shear stress}}{\text{inertia stress}} = \frac{\tau_s}{(1/2)\rho u_y^2} = f \tag{13}$$

The force exerted by fluid during a motion in a pipe is expressed by shear stress and dynamic pressure-loss by definition, i.e.

$$F_r = \tau_s \pi D L = \Delta P_{\text{loss}} \frac{\pi D^2}{4} \tag{14}$$

By combining Eqs. (13) and (14), the wall friction loss is expressed in the most frequently available form as follows:

$$\Delta P_{\text{loss}} = 2\rho u_y^2 f\left(\frac{L}{D}\right) \tag{15}$$

Additionally, there is a friction loss due to geometrical effects such as fittings or valves. In the gas manifolds of fuel-cell stacks, there are some geometrical effects not from fittings or valves but from the flange-shape structure at the junction of the manifold axial flow and each cell channel flow. A schematic illustration of the structure used in the stack considered in this study is given in Fig. 3.

Such a geometrical effect is generally estimated from the inertia force multiplied by an empirical constant (K_f) which
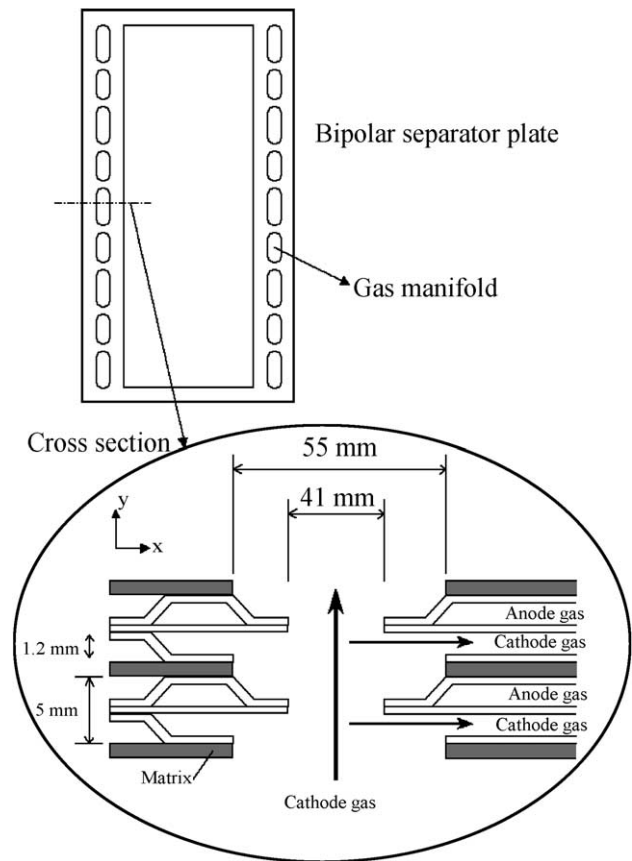

Fig. 3. Shape of manifold holes in bipolar plates of a molten carbonate fuel-cell stack.

is known for various types of fittings or valves. The combined friction loss (wall + geometry) is then obtained as a function of linear velocity, namely:

$$l_{wf} = \text{wall friction loss} + \text{fitting loss} = 2u_y^2 f\left(\frac{L}{D}\right) + K_f \frac{u_y^2}{2} \tag{16}$$

The overall mechanical balance is now expressed with an equivalent length of manifold holes from cell to cell (L_e) and a hydraulic diameter (D_H), i.e.

$$\frac{\Delta u_y^2}{2} + g\Delta h + \frac{\Delta P}{\rho} = 2u_y^2 f\left(\frac{L_e}{D_H}\right) + K_f \frac{u_y^2}{2} \tag{17}$$

The potential energy change term ($g\Delta h$) can be ignored as it is usually smaller than the others by an order of magnitude at least. In inlet gas manifolds, the kinetic energy term (Δu_y^2) contributes a negative value of pressure drop which indicates pressure recovery. This occurs when the mass flow in inlet manifolds is reduced from the feeding plate to the end plate, which result in an increase in linear velocity. When the friction loss is relatively small compared with the pressure recovery, the overall ΔP is negative and pressure increases along the main flow direction of the inlet manifolds. The reverse is true when there is a relatively large friction loss.

The equation at each junction of the manifolds is shown below. This equation can apply for both inlet and outlet manifolds by replacing the pressure term (P) by P_{in} or P_{out}, i.e.

$$\begin{aligned}\frac{\Delta P(i)}{\rho} &= \frac{P(i) - P(i-1)}{\rho} \\ &= \frac{u_y(i-1)^2 - u_y(i)^2}{2} + 2fu_y(i)^2\left(\frac{L_e}{D_H}\right) + K_f \frac{u_y(i)^2}{2} \end{aligned} \tag{18}$$

While the gas-flow in the cell channel is mostly in the laminar region, gas-flow in manifolds can be either laminar or turbulent. The coefficient of wall friction loss can be obtained from a known correlation [11]:

$$f = \frac{16}{Re}, \quad Re < 2100 \text{ (Laminar flow)} \tag{19}$$

$$f = 0.079\,Re^{-0.25},$$
$$Re > 2100 \text{ (Blasius equation for turbulent flow)} \tag{20}$$

2.4. Solution algorithm

The calculation starts with an initially guessed set of cell flow rates, $q_x(i)$. The easiest way to start is with an equally-divided cell flow rate, i.e. the feed flow rate divided by the number of cells. With a given set of cell flow rates, the cumulative local flow rates in manifolds, $Q_{in}(i)$ and $Q_{out}(i)$, are obtained from Eqs. (2), (5) and (7). Local velocities in

manifolds are obtained from the flow rates and these are then used to calculate the pressure-change in the outlet manifolds from Eq. (18) and the local dynamic pressure in the outlet manifolds ($P_{out}(i)$) from Eqs. (6) and (8). The next step is to calculate $P_{in}(i)$ from the $(N-1)$ relations for $P_{in}(i)$ and $u_y(i)$ (Eq. (18)). Since there are only $(N-1)$ equations for N pressure variables, it is necessary to specify one local pressure value at the inlet manifolds. This is called the reference inlet pressure, $P_{in}(\text{ref})$, and is easily obtained from the pressure drop in a reference cell, $\Delta P_x(\text{ref})$. The reference cell can be chosen arbitrarily. Here, No. 1 cell (top of the stack) is taken as the reference.

Examination of the variables and equations reveals that there are more equations for pressure than for flow rate. It is therefore useful to define a parameter which utilizes a redundant set of pressure equations. A basic solution strategy is then to use this parameter for adjustment of cell flow rates and continue until convergence reaches. Here, the redundant parameter is defined as:

$$\alpha(i) = \frac{P_{in}(i) - P_{out}(i)}{\Delta P_x(\text{ref})} \tag{21}$$

where $\Delta P_x(\text{ref})$ is the pressure drop in the reference cell. When all the flows in cells are equal, the $\alpha(i)$ values are all unity. A large deviation of $\alpha(i)$ values from cell-to-cell means the total gas flow is not uniformly distributed to cells. Therefore $\alpha(i)$ may be called a 'flow distribution factor'.

Some adjustment correlation is needed to make a better guess for the next calculation in each iteration step. The adjustment correlation is developed from the definition of the flow distribution factor, namely:

$$\sum_{i=1}^{N} \alpha(i) = \frac{1}{\Delta P_x(\text{ref})} \sum_{i=1}^{N} [P_{in}(i) - P_{out}(i)] \tag{22}$$

By substituting the pressure drop terms, $P_{in}(i) - P_{out}(i)$ in Eq. (22) by the equation for cell flow rate (Eq. (11)) the following formula is obtained for a new value of the pressure drop in the reference cell:

$$\Delta P_x^{new}(\text{ref}) = \frac{Q_F}{\sum_{i=1}^{N} \alpha(i)} \frac{1}{A_x} \frac{\eta L_x}{k} \tag{23}$$

With this new value of pressure drop in the reference cell, the inlet manifold pressure values are all adjusted. The flow distribution factor should be adjusted as well. New cell flow rates are then calculated from the adjusted inlet manifold pressure values. Note that, the outlet manifold pressure is not adjusted because the exit pressure is known and is equivalent to the outlet reference pressure. Once new cell flow rates are determined, they are compared with the initial guess or the previously calculated cell flow rates. The calculation continues with a new set of cell flow rates until the $q_x(i)$ values are close to the old values within an error limit. The entire solution algorithm is summarized in Appendix A.

3. Experimental

The gas pressure from a 10-cell MCFC stack was measured. The cell size was 55 cm length and 110 cm width which resulted in an active cell area of 6050 cm^2. The cell component materials and other specifications have been discussed elsewhere [12]. The fuel and oxidant gases were fed through internal gas manifolds. Both the cathode and anode gas streams flow in the same direction from the inlet to the outlet (co-flow). The overall gas-flow pattern is a reverse type (U-shape). The gas pressure was measured from inlet and outlet headers of the stack at different gas-flow rates. The overall plane view of separator plates and a schematic view of the manifold cross-section are shown in Fig. 3.

4. Results and discussion

4.1. Pressure drop across gas channels in cell area

The measured gas pressure drop is plotted as a function of flow rate in Fig. 4. The cathode and anode plates have the same geometrical structure with the same dimensions. It is therefore reasonable that the pressure-drop data for the anode and the cathode in Fig. 4 are almost identical. Linear fitting of data results in two close straight lines for the anode and the cathode, respectively. The small difference between the anode and cathode lines is probably a result of other effects such as different gas viscosity and different electrode materials. The linear behavior of pressure drop indicates that the gas-flow is in the laminar region. It should be noted that the data was obtained from a 10-cell stack. Though the data were measured between inlet and outlet headers that preserve the effect of manifold pressure, the effect of gas pressure-change in manifolds should not be significant in

Fig. 4. Pressure drop across cell channels measured from 55 cm length MCFC cells.

this short stack of only 10-cells. The pressure drop in Fig. 4 is caused mostly by the flow resistance in cell channels, ΔP_x. From the relation based on Darcy's law, the permeability can be used to characterize the flow resistance in cell channels. The permeability for anode and cathode cell channels was calculated from the data, and the results are listed in Table 1. The values for the anode and cathode are very close, as expected.

When a stack is composed of much more than 10-cells, the pressure-change in the manifolds may become significant given the size and shape of the manifold. While a short stack is easy to set up and test, a stack with a large number of cells is always difficult to test. The pressure drop from the cell channels can be measured even with a single cell, and therefore it is relatively easy to determine the flow resistance of the cell channels, as undertaken in this study. The pressure-change in the manifolds of a large stack is possible, but costly. In the next section, the manifold flow is described with the flow model (Eq. (18)) and local pressure values are predicted. A stack model with 100-cells, each with an identical size of active area to the 10-cell stack described above, is formulated. It should be considered a scale-up from 10 to 100-cells. Since the active cell area is the same, the flow resistance from the 10-cell stack data applies for cell channels of a 100-cell stack. Thus, it is possible to investigate the change of pressure in manifolds and its effect on flow distribution. Both reverse and parallel flow types are considered. Cells are numbered from the highest to the lowest (see Fig. 2). The feed gas enters the lowest plate (Nth), and the exhaust gas exits from the Nth plate in a reverse flow and from the 1st plate in a parallel flow, as shown in Fig. 2. The specification of this stack and the simulation conditions are summarized in Table 1.

4.2. Analysis of flow in manifolds

The manifold flow model developed in this study (Eq. (18)) is a relation between manifold gas pressure (P) and velocity (u_y) with irreversible pressure-loss characterized by a wall friction loss coefficient (f) and a geometrical loss coefficient (K_f). Besides the two pressure-loss terms, the kinetic energy change term also influences pressure-change in manifolds because mass change occurs at the junction of the manifold and the cell channels. The effect of such a kinetic energy change is pressure recovery in inlet manifolds and pressure-loss in outlet manifolds. Therefore, there are three different contributions to pressure-change in manifolds, as noted in Eq. (24). The wall friction loss is a pressure drop caused by viscous stress to the smooth walls of the flow length. The pressure recovery is related with mass flow change and, consequently, velocity change. The geometrical loss exists because manifold holes are not exactly straight pipes with smooth walls. Thus,

$$\Delta P_{\text{manifolds}} = \Delta P_{\text{mass change}} + \Delta P_{\text{friction loss}}$$
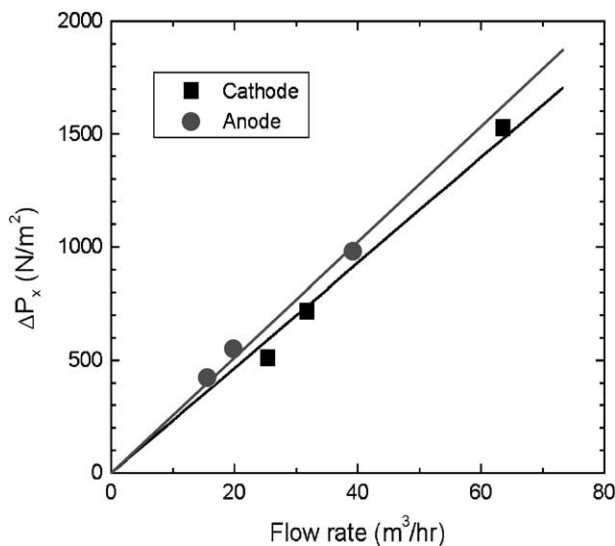$$= \Delta P_{\text{mass}} + \Delta P_{\text{wall}} + \Delta P_{\text{geo}} \qquad (24)$$

Table 1
Specification of stack and its standard operating conditions

Variable	Value
Number of cells	100
Gas-flow type	Reverse (U) or parallel (Z)
System total pressure (atm)	3
Stack heating temperature (°C)	650
Electrode size	0.55 m × 1.10 m
Effective gas channel depth (m)	0.0012
Cell-to-cell distance in manifold axis (m)	0.005
Base load current density (mA cm^{-2})	125
Cathode gas O_2 utilization	0.3
Anode gas H_2 utilization	0.8
Cathode inlet gas composition	$O_2/N_2/CO_2$ = 15/55/30
Anode inlet gas composition	$H_2/CO_2/H_2O$ = 72/18/10
Cathode molar feed flow rate per cell (mole s^{-1})	0.0432
Anode molar feed flow rate per cell (mole s^{-1})	0.00675
Cathode gas viscosity (kg m^{-1} s^{-1})	3.6×10^{-5}
Anode gas viscosity (kg m^{-1} s^{-1})	2.9×10^{-5}
Cathode gas density (kg m^{-3})	1.41
Anode gas density (kg m^{-3})	0.54
Cathode gas permeability in cell channel (m^2)	1.863×10^{-8}[a]
Anode gas permeability in cell channel (m^2)	1.616×10^{-8}[a]
Number of cathode gas manifold holes	5 holes (inlet) → 4 holes (outlet)
Number of anode gas manifold holes	4 holes (inlet) → 5 holes (outlet)
Hydraulic diameter of cathode manifold holes	0.0786 m (inlet) → 0.0691 m (outlet)
Hydraulic diameter of anode manifold holes	0.0691 m (inlet) → 0.0786 m (outlet)

[a] Obtained based on data of Fig. 4.

The pressure-change due to the mass change (ΔP_{mass}) is a reversible energy change caused by different gas velocities before and after the junction of manifolds. The pressure-loss due to wall friction (ΔP_{wall}) is estimated with a wall friction loss coefficient from correlation (Eqs. (19) and (20)). The pressure-loss due to geometrical effect (ΔP_{geo}) is estimated with a geometrical coefficient. Though some geometrical pressure-loss coefficients are available for various fittings or valves, none fit a specific shape of gas-flow manifolds such as that shown in Fig. 3. The shape of the manifold junction can be approximated to some known types of fitting or valve. In Table 2, several different cases of approximation are suggested and K_f values are compared [13]. There are also different approaches to calculate pressure and flow distribution for other types of application of manifolds [14].

A typical plot of Reynolds number versus cell number is shown in Fig. 5. The y-coordinate is plotted in a logarithmic

scale. When the plot is made in a linear scale, it is almost linear with the variation of Re in the cells. Though Fig. 5 shows the case of a reverse flow only, the Reynolds number in a parallel flow is qualitatively the same for Re_{in} and Re_x, while Re_{out} should be symmetrical with respect to the center-height cell plane (50th). The range of Reynolds numbers for cell channel flow (Re_x) is below the order of 10^2 in Fig. 5 and is certainly in the laminar flow region. The range of Reynolds numbers for manifold flow is placed in both the laminar and turbulent regions. The manifold flow curves

Table 2
Geometrical pressure-loss coefficients from different approximations [13]

Geometry	K_f formula	K_f value[a]
Straight pipe	0.0	0.0
Rounded entrance	0.05	0.05
Sudden contraction	$0.45 (1 - \beta)$	0.2
Fully-open gate-valve	0.2	0.2
Orifice (sharp-edge)	$2.7 (1 - \beta) (1 - \beta^2) (1/\beta^2)$	2.679

Here β = (smaller cross-sectional area)/(larger cross-sectional area).
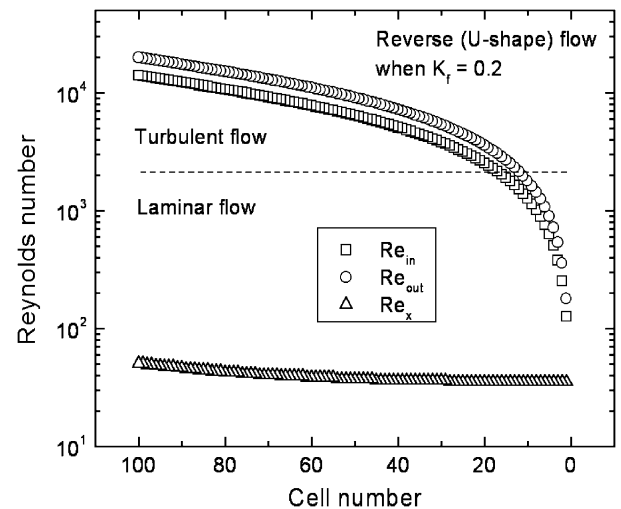[a] For fuel-cell stack in this study, $\beta = 0.556$.

Fig. 5. Comparison of Reynolds number in cell channel area and manifolds.

cross the line of criterion for flow type ($Re = 2100$) at a cell number of about 10–20. This means that turbulent flow is expected if the number of cells exceed 20 in this stack configuration and manifold design. For laminar flow, the pressure drop is linearly proportional to the gas velocity and this usually creates a less significant pressure-change compared with turbulent flow where the pressure drop is amplified with increasing velocity, for example (velocity)$^{1.75}$ from the Blasius equation. For a 100-cell stack, much of the manifold flow is turbulent and this will create a larger pressure drop than for laminar flow.

4.3. Pressure-loss and recovery in manifolds

With the K_f values in Table 2, the flow model is solved according to the algorithm shown in Appendix A. The three pressure-change terms in Eq. (24) are plotted for inlet manifold as a function of cell number in Fig. 6. A positive ΔP indicates pressure-loss, whereas a negative ΔP indicates pressure recovery. When there is no geometrical effect ($K_f = 0$), the pressure-loss is negligible compared with the pressure recovery caused by mass decrease in inlet manifolds (Fig. 6a). As K_f increases (Fig. 6a–d), the magnitude of the geometrical pressure-loss increases dramatically while the magnitude of the pressure recovery shows only a small increase. Pressure-loss by wall friction is always much smaller than both the other effects regardless of the value of K_f. The two dominant contributions of pressure-change in manifolds are obviously from mass change and geometry, and their relative influence depends greatly on geometrical shape that determines a K_f value.

The data in Fig. 6 demonstrate how manifold geometry affects the flow in manifolds. The loss coefficient of 0.2 is for a fully-open gate-valve that has a relatively smaller flow resistance compared with most other fittings or valves. Despite such a relatively small geometrical flow resistance,
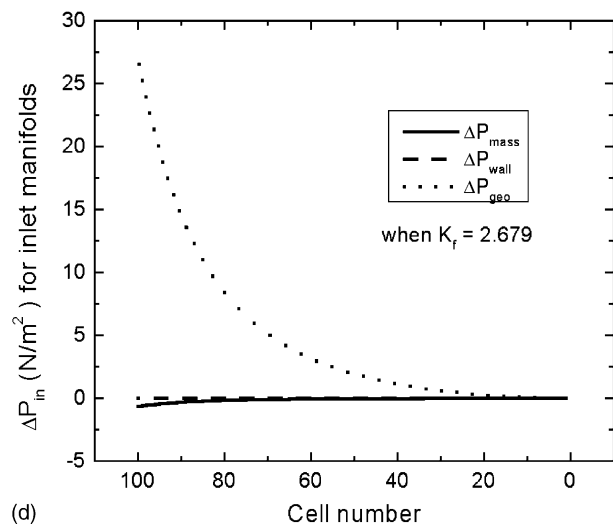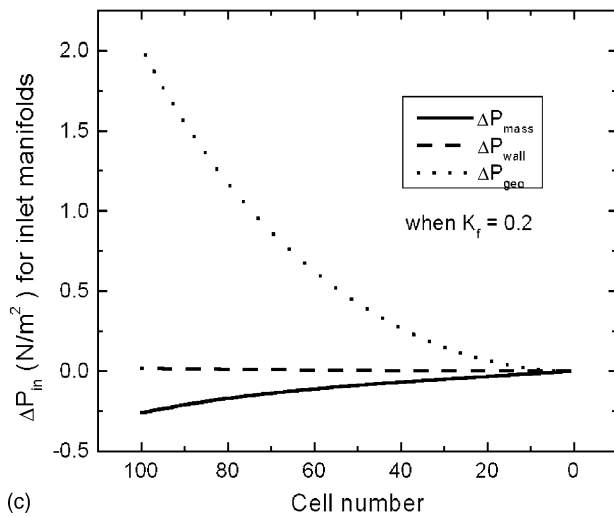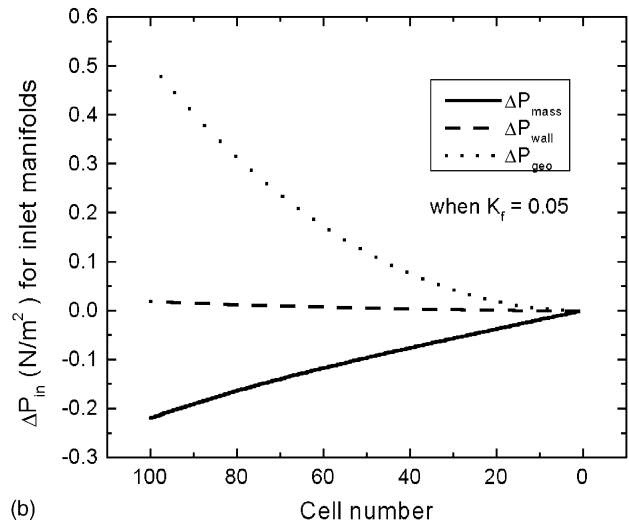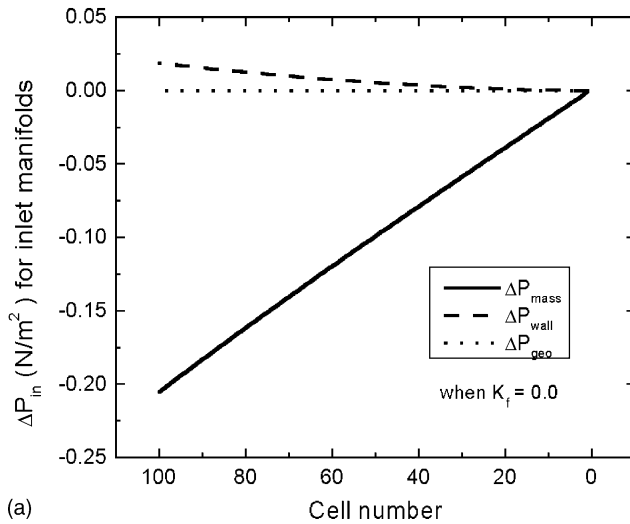

Fig. 6. Analysis of pressure-loss and recovery in inlet manifolds at different values of geometrical pressure-loss coefficient: (a) $K_f = 0.0$; (b) $K_f = 0.05$; (c) $K_f = 0.2$; (d) $K_f = 2.679$.

its effect on the distribution of manifold pressure is significant, as shown in Fig. 6. This explains why the manifold is a crucial part in the design of large-scale fuel-cell stacks.

It is most difficult to determine the K_f value, since fuel-cell stacks can be designed in many different ways. Because flow resistance must be affected by both the structure and the size of the stack, it is safe to assume that every stack has a different flow resistance in the manifolds and, therefore, a different K_f value. If we take an example from Fig. 3, there are no smooth walls in the gas-flow through manifolds. These manifold holes are more like pipes with rough surfaces on the walls and with a series of many orifices in the flow direction. Though some pressure-loss coefficients are available in literature, most of them are for flow in pipes with smooth walls and for very well-described geometry. The manifold shape can still be assumed to be one of the known geometry types of fittings or valves, but some precision of the model may have to be sacrificed when such approximations are made.

4.4. Overall pressure variation in manifolds

Combining the pressure drop in cell channels and each contribution of pressure-change in inlet and outlet manifolds, the overall pressure distribution profiles along the gas-flow path in the stack is obtained, shown in Fig. 7. For comparison, the plots are made for the cases of $K_f = 0.0$ and 0.2. Both reverse and parallel flows are considered for each K_f value. When there is no geometrical pressure-loss ($K_f = 0.0$), there is virtually no noticeable change in pressure from cell-to-cell, i.e. the pressure curves are almost flat (Fig. 7a and b). More careful examination, however, reveals that the inlet and outlet pressure curves are both increasing in parallel in a reverse flow (Fig. 7a) and diverge from the lowest cell No. (100) to the highest cell No. (1) in a parallel flow (Fig. 7b). When there is some contribution from the geometrical effect ($K_f = 0.2$), the inlet and outlet pressure curves more clearly converge from the lowest to the highest cell in a reverse flow (Fig. 7c), and decrease in parallel in a
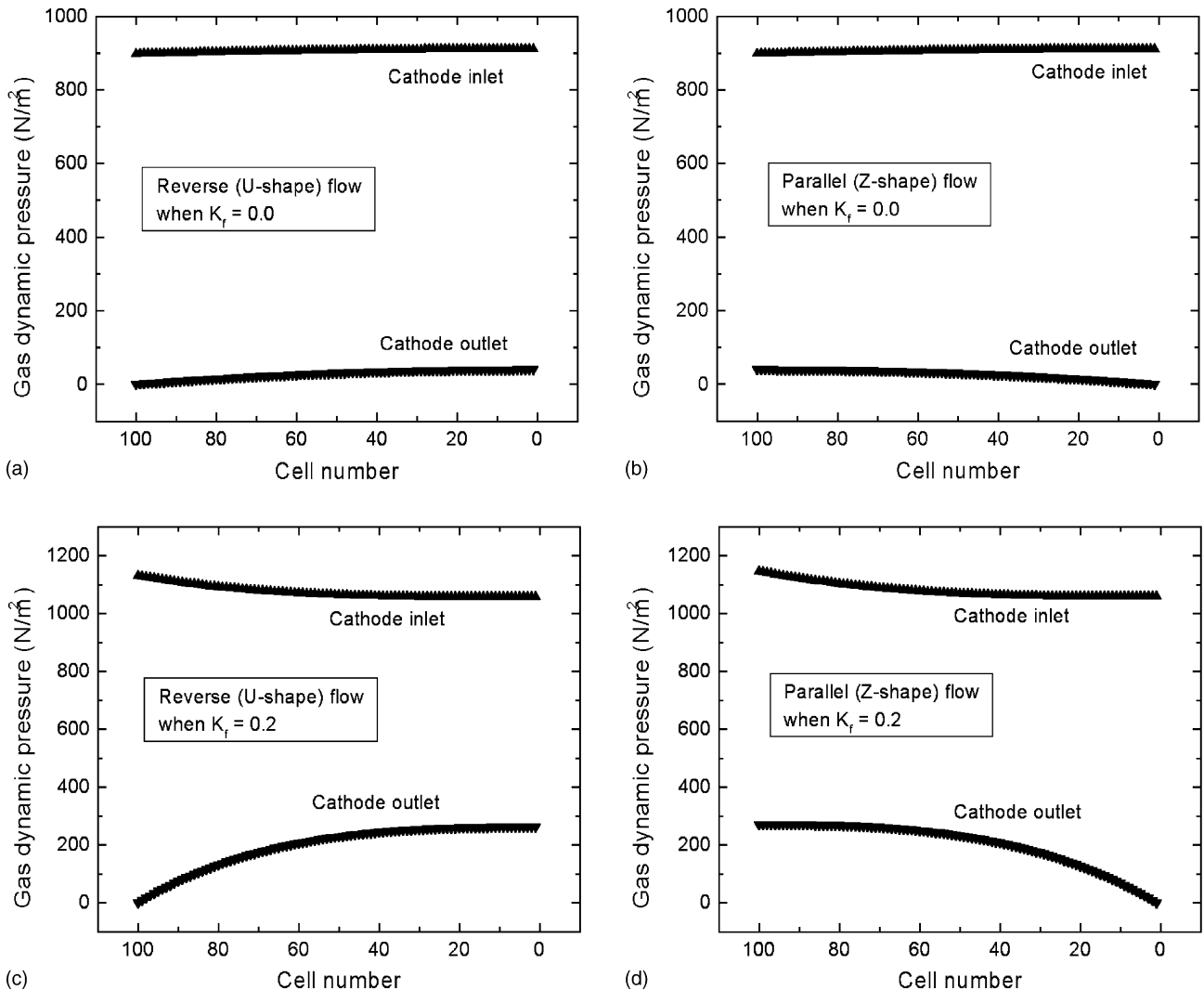

Fig. 7. Overall pressure distribution in 100-cell fuel-cell stack: (a) reverse flow with $K_f = 0.0$; (b) parallel flow with $K_f = 0.0$; (c) reverse flow with $K_f = 0.2$; (d) parallel flow with $K_f = 0.2$.

parallel flow (Fig. 7d). These four different pressure curves describe most general types of pressure distribution in the manifolds of fuel-cell stacks. The slope of each pressure curve will change as either the manifold size or the manifold shape changes.

Prediction of pressure curves is important, as flow distribution into cells is directly related to pressure variation. For the 100-cell MCFC stack considered in this study, lowering the pressure-loss (lower K_f) appears most beneficial because Fig. 7 implies there is almost even pressure distribution at $K_f = 0.0$. This stack apparently has manifold holes that are sufficiently large to prevent significant pressure recovery or drop from mass change. In general, it is more desirable to have parallel curves of inlet and outlet pressure because the flow rate at the ith cell ($q_x(i)$) is proportional to the pressure difference between inlet and outlet.

4.5. Flow distribution in cells

From the pressure variation in the manifolds, the mass flow to each cell is calculated. The overall flow distribution with various geometrical loss coefficients in a reverse flow stack is presented in Fig. 8. In this plot, each cell flow rate is divided by the average flow rate over 100-cells. Even though it is not possible to confirm which K_f value would best approximate the manifold flow resistance, at least an indication is given of the flow distribution and the extent to which it can change with increasing flow resistance. The pressure curves of Fig. 7 show that the flow distribution is very uniform in the complete absence of a geometrical effect. The maximum and minimum flow deviation is less than 4% from the average, in the case of $K_f = 0$. The flow distribution with increasing geometrical effect is still reasonably acceptable until $K_f = 0.2$. At $K_f = 0.2$, the maximum flow deviation is about 30% from the average and the minimum flow deviation is less than 10% from the average. Obviously, the
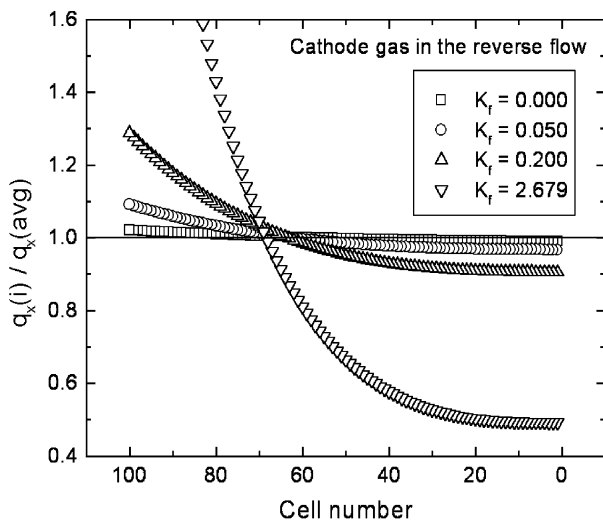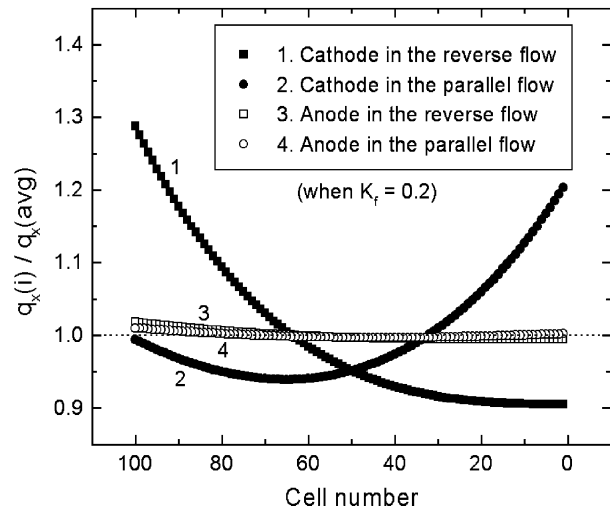

Fig. 9. Comparison of flow distribution to cells in reverse flow and parallel flow for cathode and anode gases under standard stack operating condition with $K_f = 0.2$.

situation of $K_f = 2.679$ has to be avoided since it results in a poorly distributed gas-flow. If some data are available to make a close approximation of K_f, then the flow distribution can be predicted from the data in Fig. 8. If there are no experimental data for K_f and there is a need to design a large-scale stack, an extreme case of non-even flow distribution may have to be considered.

The overall flow distribution in a reverse flow and in a parallel flow are compared in Fig. 9 for an equal number of cells and sizes for $K_f = 0.2$. This value of K_f was chosen because it appears to represent a fairly moderate flow resistance among the approximations listed in Table 2. Although, the two types of flow display different shapes of distribution curve, neither appears to be better than the other in terms of flow uniformity. In this stack, it is clearly less important whether the overall gas-flow is a U- or Z-shape. Rather, a better flow distribution is obtained by reducing the geometrical flow resistance. This is true only for the specific case selected in this study. In some other stack designs, it is possible that either a reverse flow or a parallel flow has more benefits over other flow types in terms of better flow distribution.

The distribution of the cathode and anode gas-flows in the selected fuel-cell stack are also presented in Fig. 9. As shown in Table 1, the anode gas-flow rate is much lower than the cathode flow rate due to the high utilization of fuel. Because of its relatively low total flow rate, gas velocities are much lower in anode gas manifolds than in cathode gas manifolds. The change of pressure in manifolds is therefore much less significant at the anode than at the cathode, and this results in an overall uniform flow distribution in the anode. In general, the flow rate entering each cell should be larger than a minimally required flow rate. The latter is the rate of fuel supply to the anode or oxygen supply to the cathode that is completely utilized for a desired current load. The size of the manifolds should be designed carefully so

Fig. 8. Flow distribution to cells at different values of geometrical pressure-loss coefficient.

that cell flow rates are all above the minimum requirement. The fuel-cell stack chosen for this study was designed satisfactorily for its standard operation.

5. Conclusions

A general model for the calculation of pressure and flow distribution in fuel-cell stacks has been proposed in this study. It is emphasized that pressure variation in fuel-cell stack manifolds is influenced not only by manifold size but also by manifold geometry. The effect of manifold geometry can be modeled with additional pressure-losses to that experienced with a straight smooth wall. The pressure-loss caused by fittings or valves in the pipe flow can be estimated, but it is more desirable to determine a geometrical loss coefficient from experimental measurements as it must be assumed that each fuel-cell stack has its unique design of manifold.

The manifold flow model combined with cell channel flow has been proposed to predict the pressure variation and flow distribution for a 100-cell MCFC stack. The results show that the gas-flow in cell channels is in the laminar region while the gas-flow in manifolds is mostly turbulent. When the geometry of the manifold flow junction of this fuel-cell stack is modeled as a fully-open gate-valve or sudden contraction with a geometrical loss coefficient of 0.2, certain non-uniformity of the flow distribution is observed in either a reverse flow (U-shape) or a parallel flow (Z-shape). The non-uniform distribution is more significant at the cathode where a large amount of excess gas enters the stack, than at the anode where gas utilization is sufficiently high to allow a relatively small amount of total gas flow. Overall, the model predicts that the cell flow rates are within a reasonably acceptable range for operation of the chosen stack at its standard condition. It has been demonstrated how the manifold design can be evaluated from engineering models and can be improved further in this study.

Appendix A. Algorithm for calculation of pressure and flow distributions in fuel-cell stacks

Step 1: Initial guess of cell flow rates and a reference inlet pressured drop

$$q_x(i) = \frac{Q_F}{N}, \quad (i = 1 \text{ to } N) \tag{A.1}$$

$$\Delta P_x(\text{ref}) = \frac{Q_F}{N} \frac{1}{A_x} \frac{\eta L_x}{k}, \quad (\text{ref} = 1) \tag{A.2}$$

Step 2: Calculate flow rates and linear velocity in manifolds and Reynolds numbers

$$Q_{\text{in}}(i) = \sum_{j=1}^{i} q_x(j), \quad (i = 1 \text{ to } N) \tag{A.3}$$

$$Q_{\text{out}}(i) = \sum_{j=1}^{i} q_x(j), \quad \text{for reverse flow}$$

$$Q_{\text{out}}(i) = \sum_{j=1}^{N} q_x(j), \quad \text{for parallel flow} \tag{A.4}$$

$$u_x(i), \, u_{\text{in}}(i), \, u_{\text{out}}(i), \, Re_x(i), \, Re_{\text{in}}(i), \, Re_{\text{out}}(i)$$

Step 3: Calculate outlet manifold pressure

$$P_{\text{exit}} = 0 \tag{A.5}$$

$$\frac{\Delta P_{\text{out}}(i)}{\rho} = \frac{u_{\text{out}}(i-1)^2 - u_{\text{out}}(i)^2}{2}$$
$$+ \left(2f\frac{L_e}{D_H} + \frac{K_f}{2}\right)u_{\text{out}}(i)^2, \quad (i = 2 \text{ to } N) \tag{A.6}$$

$$P_{\text{out}}(i-1) = P_{\text{out}}(i) + \Delta P_{\text{out}}(i), \quad \text{for reverse flow}$$

$$P_{\text{out}}(i) = P_{\text{out}}(i-1) + \Delta P_{\text{out}}(i), \quad \text{for parallel flow} \tag{A.7}$$

Step 4: Calculate inlet manifold pressure

$$P_{\text{in}}(\text{ref}) = \Delta P_x(\text{ref}) + P_{\text{out}}(\text{ref}), \quad (\text{ref} = 1) \tag{A.8}$$

$$\frac{\Delta P_{\text{in}}(i)}{\rho} = \frac{u_{\text{in}}(i-1)^2 - u_{\text{in}}(i)^2}{2}$$
$$+ \left(2f\frac{L_e}{D_H} + \frac{K_f}{2}\right)u_{\text{in}}(i)^2, \quad (i = 2 \text{ to } N) \tag{A.9}$$

$$P_{\text{in}}(i) = P_{\text{in}}(i-1) + \Delta P_{\text{in}}(i) \tag{A.10}$$

Step 5: Calculate flow distribution factors

$$\alpha(i) = \frac{P_{\text{in}}(i) - P_{\text{out}}(i)}{\Delta P_x(\text{ref})}, \quad (i = 1 \text{ to } N) \tag{A.11}$$

Step 6: Calculate a new value of reference pressure drop

$$\Delta P_x^{\text{new}}(\text{ref}) = \frac{Q_F}{\sum_{i=1}^{N} \alpha(i)} \frac{1}{A_x} \frac{\eta L_x}{k} \tag{A.12}$$

Step 7: Adjust inlet manifold pressure from new reference pressure drop

$$P_{\text{in}}^{\text{adj}}(\text{ref}) = \Delta P_x^{\text{new}}(\text{ref}) + P_{\text{out}}(\text{ref}), \quad (\text{ref} = 1) \tag{A.13}$$

$$P_{\text{in}}^{\text{adj}}(i) = P_{\text{in}}(i-1) + \Delta P_{\text{in}}(i), \quad (i = 2 \text{ to } N) \tag{A.14}$$

Step 8: Adjust flow distribution factors from new reference pressure drop and adjusted inlet manifold pressure

$$\alpha^{\text{adj}}(i) = \frac{P_{\text{in}}^{\text{adj}}(i) - P_{\text{out}}(i)}{\Delta P_x^{\text{new}}(\text{ref})}, \quad (i = 1 \text{ to } N) \tag{A.15}$$

Step 9: Calculate new set of cell flow rate from adjusted inlet manifold pressure

$$q_x^{\text{new}}(i) = [P_{\text{in}}^{\text{adj}}(i) - P_{\text{out}}(i)]\frac{k}{\eta L_x}A_x, \quad (i = 1 \text{ to } N) \tag{A.16}$$

Step 10: Check convergence

$$ERR = \sum_{i=1}^{N} \left[\frac{q_x^{new}(i) - q_x(i)}{q_x(i)} \right]^2 \tag{A.17}$$

If $ERR > \epsilon$, update $\Delta P_x(ref)$ and $q_x(i)$ and go to Step 2. If $ERR < \epsilon$, stop.

References

[1] M. Hishinuma, T. Kawashima, I. Yasuda, Y. Matsuzaki, K. Ogasawara, in: U. Bossel (Ed.), Proceedings of the First European Solid Oxide Fuel-Cell Forum, European SOFC Forum Secretariat, Baden, Switzerland, 1994, p. 953.

[2] P. Costamagna, E. Arato, E. Achenbach, U. Reus, J. Power Sources 52 (1994) 243.

[3] G. Belmonte, M. Chindemi, A. Malandrino, M. Mancini, in: U. Bossel (Ed.), Proceedings of the First European Solid Oxide Fuel-Cell Forum, European SOFC Forum Secretariat, Baden, Switzerland, 1994, p. 327.

[4] H. Hirata, M. Hori, J. Power Sources 63 (1996) 115.

[5] R.J. Boersma, N.M. Sammes, J. Power Sources 63 (1996) 215.

[6] R.J. Boersma, N.M. Sammes, J. Power Sources 66 (1997) 41.

[7] E. Achenbach, U. Reus, in: S.C. Singhal, M. Dokiya (Eds.), Proceedings of Sixth International Symposium on Solid Oxide Fuel-Cells (SOFC VI), Electrochemical Society, Pennington, NJ, USA, 1999, p. 1125.

[8] P. Argyropoulos, K. Scott, W.M. Taama, J. Appl. Electrochem. 30 (8) (2000) 899.

[9] H. Hirata, T. Nakagaki, M. Hori, J. Power Sources 102 (2001) 118.

[10] J.H. Koh, B.S. Kang, H.C. Lim, AIChE J. 47 (9) (2001) 1941.

[11] C.O. Bennett, J.E. Myers, Momentum, Heat and Mass Transfer, 3rd ed., McGraw-Hill, New York, 1982.

[12] H.C. Lim, B.S. Kang, H.K. Seo, K.S. Ahn, C.G. Lee, J.H. Koh, Y.S. Yoo, S.A. Hong, in: Proceedings of the 2000 Fuel-cell Seminar, Portland, Oregon, USA, 2000, p. 683.

[13] R.B. Bird, W.E. Stewart, E.N. Lightfoot, Transport Phenomena, Wiley, New York, 1960.

[14] J.J. McKetta (Ed.), Piping Design Handbook, Marcel Dekker, Inc., New York, 1972.